Simulation of Two-Transistor Parallel and Series Circuits for Gas Sensing Validated by Experimental Data

W. Wondmagegn[a] , Yingli Chu[b], Hui Li[b], Howard E. Katz[b], Jia Huang[c]

[a]Electrical and Computer Engineering Department, The College of New Jersey, NJ 08628, USA,
[b]Department of Materials Science and Engineering, Johns Hopkins University, Baltimore, MD 21218, United States
[c]School of Materials Science and Engineering, Tongji University, Shanghai, 201804, P.R. China

Corresponding Author: W. Wondmagegn, *E-mail:* wondmagw@tcnj.edu

Abstract
Organic field effect transistors (OFETs) in parallel and series circuit configurations are simulated and tested for gas sensing activity. The devices are based on PQT12 and PQTS12 organic semiconductor thin films. Two-dimensional finite element simulation methodology is implemented. It is assumed that traps due to defects and grain boundaries are uniformly distributed throughout the semiconductor film. Gaussian trap distributions are used in the simulation. Gas sensing is accounted for by a doping-dependent hopping mobility model in the organic active material. Interface traps and charges at the interface between the polymer channel and gate insulator are incorporated. Transistors in both parallel and series configurations are studied. Compared to individual OFET-based sensors, the circuit configuration achieves significantly increased sensitivity to analyte, as indicated by the simulation and in agreement with experimental observations. This supports the concept of combining transistors to enhance analyte sensitivity, and provides a method for advance screening of combinations of OFETs for high signal-to-drift ratios. The absolute value of drain currents for series circuits is lower than that of parallel circuits; however, the series circuits display higher analyte sensitivity.

1. Introduction

Conventionally, organic field effect transistors (OFETs) are envisioned for applications in flexible displays, electronic paper, radio frequency identification (RFID) tags, and smart cards [1-3]. A recent trend in the field includes involving organic field effect transistors in a variety of low-cost electronic gas sensing technologies for potential applications in environmental, biological, and industrial areas [4-10]. In some respects, the operation of organic electrochemical transistors (OECT) is analogous to that of conventional organic field effect transistors, though the complex interplay between ionic and electronic motion must be considered in a way that is much less applicable to OFETs [11,12]. For both OFETs and OECTs, charge carriers are injected into the channel of the transistor, by carrier injection or electrochemistry, respectively, thus changing its electrical conductivity [11]. While OFETs usually operate in accumulation mode, OECTs can be designed for either accumulation mode or depletion mode operation [11,13-15].

The main feature of disordered organic conducting materials is the strong localization of charge carriers in potential wells formed by defects and traps [16,17]. Intrinsic number densities of traps and defects ranging from 10^{18} to 10^{21} cm^{-3} is reported [18]. As a result, charge transport occurs via carrier hopping within an energetically disordered system of localized states. The hopping rate is controlled by the energy difference between the occupied deep states and the effective transport level. Published reports show that the carrier mobility in conjugated polymers depends on carrier concentration. Increasing charge carrier density will increase the mobility by filling deep traps and raising the energy distribution of occupied states [18-20]. Depending on the type and density of traps, the experimental data of OFETs have been analyzed either on the basis of the multiple trap and release model or the variable-range hopping model [21-24]. Percolation can occur through the variable range hopping within the Gaussian density of states of the highest occupied molecular orbital or lowest unoccupied molecular orbital. According to the multiple trapping and release model, charge transport is controlled by traps that are energetically located between highest occupied molecular orbital and lowest unoccupied molecular orbital [25-32]. Most of the charge carriers reside at trap sites and are temporarily released to the highest occupied molecular orbital or lowest unoccupied molecular orbital, depending upon the position of the trap level and temperature.

Much of the research effort in this field is focused on understanding and optimizing organic semiconductor morphology and charge transport properties through experimental iterations [11,33]. Given the wide range of applications of field effect transistor sensors, it is important to understand their underling device physics and current–voltage characteristics at a level where some of this tedious iteration can be simulated. This requires developing an accurate and comprehensive theoretical and simulation model. However, the vast majority of the theoretical work available [11,14,34-40] is limited to 1-D and equivalent circuit models with different models covering different aspects of device physics, i.e DC, steady state, and transient, to interpret experimental data in either accumulation or depletion mode. In addition to analytical modeling and simulation, physical device simulation provides better physical insights by applying fundamental semiconductor device equations such as Poisson's and continuity equations. Finally, simulations rarely if ever encompass multiple OFETs in amplifying or compensating circuits, both of which are important for achieving useful sensing signals.

In the present work, a physical simulation is presented for transistors and circuits with and without exposure to analytes. The simulation approach combines physically based modeling and parameter estimation, in which a subset of model parameters is estimated using published experimental data. The simulation results are found to be useful for interpreting conducting polymer sensor responses to NO_2 gas. The concept of combining two transistors made from different active materials could bring two-fold advantages. It could increase analyte sensitivity by combining responses of the two transistors and it could also reduce environmental

degradation effects by using materials that respond to environment effects in compensating ways. Therefore, extending the simulation to circuits is especially compelling.

2. Device Simulation

Device characteristic simulation of transistors is carried out using the drift-diffusion model. The two-dimensional device simulation is performed using Silvaco's ''ATLAS'' device simulator [41]. The device (see Figure 1) was designed with 200 μm channel length and 11 mm width. The details of fabrication and experimental characterization of the devices and circuits used in the simulation are described in reference 7.

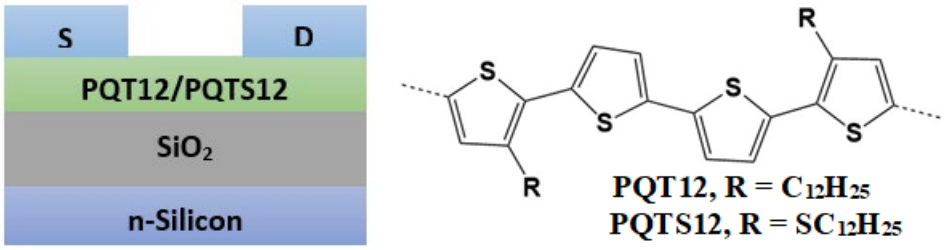

Fig. 1 *Simulated PQT12/PQTS12 Thin Film Transistor, and polymer semiconductor structures*

The work function of 5.1 eV for gold source/drain electrodes and relative permittivity of 3.7 for SiO_2 dielectric are used [42-44]. Highly n-doped Silicon with work function assumed to be a typical value of 4.15 eV [45] is used as gate electrode. Semiconductor-insulator interface charge on the order of $1.2x10^{11}$ cm^{-2} and $2x10^{10}$ cm^{-2} are used for PQT12 and PQTS12, respectively (structures shown in Fig. 1). These values are extracted from the best fit by matching simulation and experiment iteratively. The band gap and electron affinity of the polymers are determined from the UV-Vis absorbance of the PQT12 and PQTS12 films [7]. The values are 2eV and 1.8eV for PQT12 and PQTS12, respectively. Material parameters collected from literature [46,47] and used in the simulation are summarized in Table 1.

	PQT12	**PQTS12**
Band gap	2 eV	1.8eV
Affinity	3.1 eV	3.2 eV
Permittivity	3	3
Trap density	$7.1x10^{15}cm^{-3}$	$1.2x10^{16}cm^{-3}$
Polymer thickness	100 nm	100 nm
Oxide thickness and permittivity	300 nm, 3.7	300 nm, 3.7
S/D Gold thickness and wf	50 nm, 5.1 eV	50 nm, 5.1 eV
Gate, n-poly-Si thickness and wf	50 nm, 4.15 eV	50 nm, 4.15 eV
Channel length	2 mm	2 mm
Channel width	11 mm	11 mm
Interface charge	$1.2x10^{11}$ cm^{-2}	$2x10^{10}$ cm^{-2}
Attempt to jump frequency (ν_0)	$6x10^{12}$ Hz	$5.75x10^{12}$ Hz
Gamma (γ)	$1.2x10^{7}$ cm^{-1}	$1.26x10^{7}$ cm^{-1}
Beta (β),Sigmma	1.5, 0.34	1.5, 0.34

Table 1 Summary of material and model parameters used in simulations

The simulation is based on the generalized drift-diffusion equations described below [48,49],

$$Poisson\ equation: div(\varepsilon \nabla \psi) = q(n - p - N_D^+ + N_A^-) + Q_T \quad (1)$$

$$Current\ continuity\ equation: \frac{\partial n}{\partial t} = \frac{1}{q} div\vec{J}_n + G_n - R_n \quad (2)$$

$$Current\ density\ equations: \vec{J}_n = qn\mu_n\vec{E}_n + qD_n\nabla \mathrm{n} \quad (3)$$

$$\vec{J}_p = qn\mu_p\vec{E}_p + qD_p\nabla \mathrm{p} \quad (4)$$

where D_n and D_p are electron and hole diffusion coefficients respectively. G_n is electron generation rate, G_p is hole generation rate. R_n and R_p are electron and hole recombination rates, respectively. Q_T is total fixed charge.

Impurity traps are introduced to customize the drift-diffusion equations defined for crystalline semiconductors into non-crystalline organic semiconductors. It is assumed that traps are uniformly distributed throughout the film. Gaussian trap distributions are introduced in the simulation. The Gaussian distribution is described by its density of states (N_i and N_t) and its characteristic decay energy (σ_i and σ_t) as shown in equation 5 [16,41].

$$g(E) = \frac{N_i}{\sqrt{2\pi}\sigma_i} exp\left(-\frac{E^2}{2\sigma_i^2}\right) + \frac{N_t}{\sqrt{2\pi}\sigma_t} exp\left(-\frac{(E+E_t)^2}{2\sigma_t^2}\right) \quad (5)$$

Previously, PQT12 and PQTS12 polymers are reported to have equivalent uniform distributions of electron traps in the range of $1x10^{14}$ to $1x10^{16}$ cm^{-2} eV^{-1} over a wide range of trap energies [46,50]. The doping-dependent charge carrier mobility (equation 6) used in the simulation assumes the effect of trap filling on the effective transport energy (equation 7) in a hopping system with a Gaussian DOS distribution (equation 5) [16,41].

$$\mu_{tr} = \frac{q\,\nu_0}{kT}\left[\int_{-\infty}^{E_{tr}} g\,(E)dE\right]^{-2/3} exp\left[-2\left(\frac{3\beta}{4\pi}\right)^{1/3}\gamma\left[\int_{-\infty}^{E_{tr}} g\,(E)dE\right]^{-1/3}\right] \quad (6)$$

$$\int_{-\infty}^{E_{tr}} g(E)(E_{tr} - E)^3\, dE = \frac{6\beta}{\pi}(\gamma kT)^3 \quad (7)$$

where ν_0 is the attempt-to-jump frequency, $1/\gamma$ is inverse of carrier localization radius, E_{tr} is effective transport level of the energy, and β is the percolation constant.

3. Results and Discussion

3.1 Device and circuit characterization

3.1.1 Device simulation PQT12 and PQTS12

Before simulating gas analyte sensing, transistors are simulated and matched with experiment for the purpose of extracting device parameters. Figure 2 shows output characteristics and transfer curves for experimental and simulation results. In the figures, the black curves represent experimental data and the red represent simulation data. Figures 2a and b correspond to PQT12 and Figures 2c and d correspond to PQTS12 OFETs, respectively.

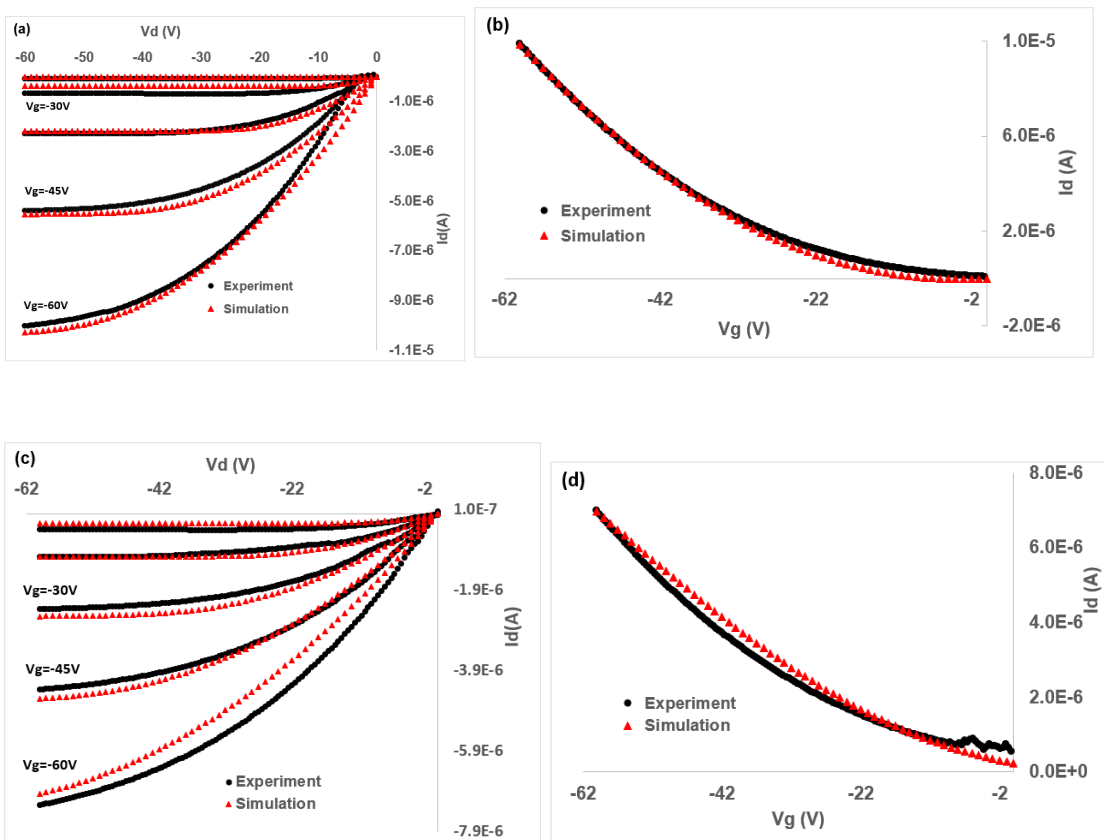

Fig.2 *(a), (b) PQT12 Id-Vd and Id-Vg curves; (c), (d) PQTS12 Id-Vd and Id-Vg curves.*

A comparison of experimental data with simulation data show good agreement for OFETs made from both polymers. Particularly for higher gate voltages, the simulations seem to overlap with experiment. Parameters extracted from simulation are trap density, interface charge density, and mobility. These parameters are listed in Table 1 and are used as initial parameters in subsequent simulations, i.e circuit and analyte sensitivity simulations.

3.1.2 Circuit simulation *– parallel and series configuration of two transistors*

Based on the material and mobility parameters validated from device simulation, listed in Table 1, two transistors are simulated in parallel and series configurations as shown in Figure 3.

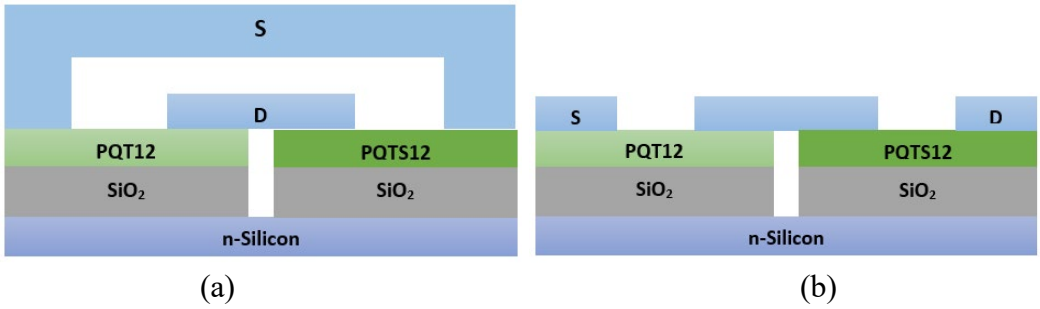

Fig.3 *(a) Parallel and (b) Series configuration of PQT12 and PQTS12 Transistors*

Parameters from single OFETs are used as a starting point and were then adjusted for best fits in the circuits. Simulation results are displayed in Figure 4. The result serves as a basis for gas analyte sensing simulation performed in section 3.2. Comparing individual device simulation (Figure 2) with the circuit simulation (Figure 4), parameters that show variations are summarized in Table 2 for parallel and series circuits, respectively.

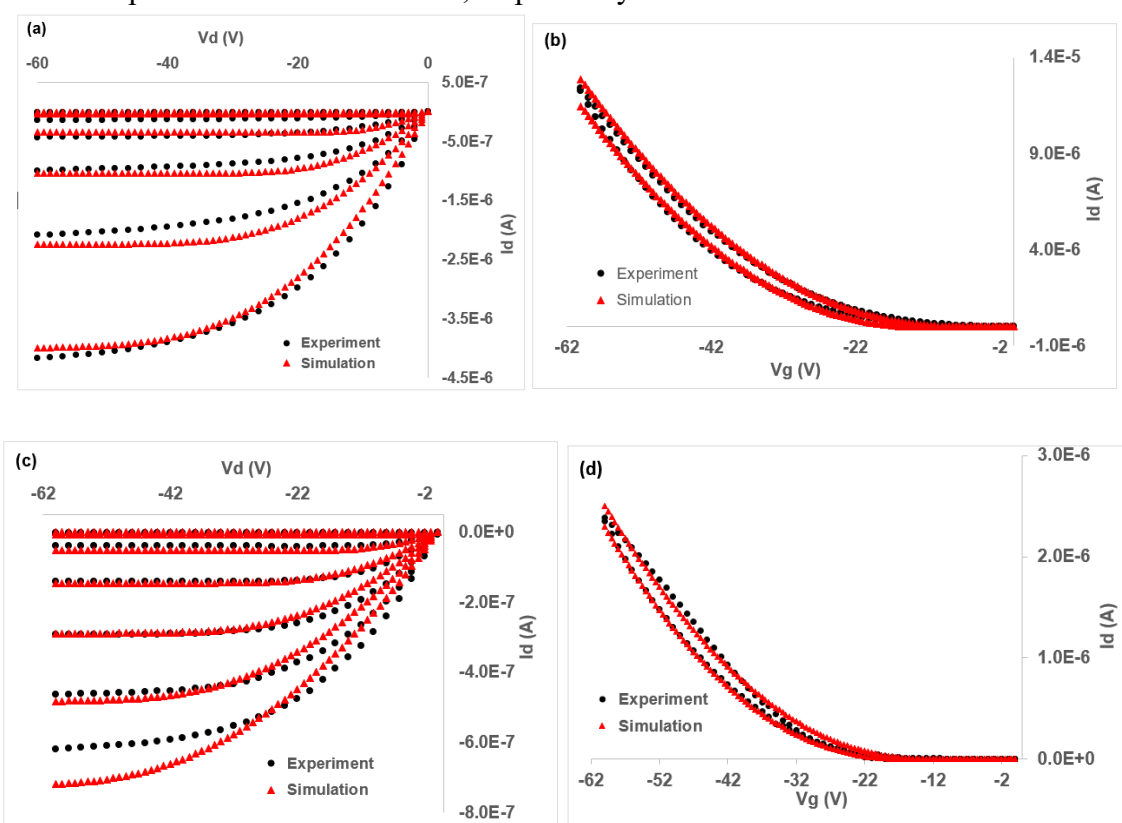

Fig.4 *(a), (b) parallel circuit Id-Vd and Id-Vg curves; (c), (d) series circuit Id-Vd and Id-Vg curves*

The table presents values of these parameters for three simulation cases. The first case is simulation for the characteristic curves of the circuits. The second and third cases present values extracted from transfer curve simulations that are matched to measurement data taken before and after the characteristic curves, respectively. As shown in Figures 4 b and d, the drain-current vs gate-voltage characterizations performed before and after the characteristic curves did not exactly overlap, indicating hysteresis effect due to charge trapping and de-trapping effects.

The circuits also operated as though they were typical p-type transistors. At the same gate bias voltage and source-drain voltage (V_d) applied to the circuits, the parallel circuit exhibited higher drain current (I_d) than the series one. The two transistors in the circuits operated at the same common gate bias, and V_d across the parallel circuit was the same voltage across each of them while V_d across the series circuit was the sum of the voltages across each transistor, which means both transistors in a series circuit operated at lower source-drain voltages, resulting in a smaller drain current.

Circuit	**Current -Voltage Characteristic**	**Material**	**Trap Density**	**Interface charge density**
Parallel	Characteristic curve	PQT12	$8x10^{15}cm^{-3}$	$7.73x10^{12}cm^{-2}$
		PQTS12	$8x10^{16}cm^{-3}$	$1.73x10^{12}cm^{-2}$
	Transfer I	PQT12	$7x10^{15}cm^{-3}$	$7.2x10^{12}cm^{-2}$
		PQTS12	$7x10^{16}$ cm^{-3}	$1.2x10^{12}cm^{-2}$
	Transfer II	PQT12	$7x10^{15}cm^{-3}$	$7.5x10^{12}cm^{-2}$
		PQTS12	$7x10^{16}cm^{-3}$	$1.5x10^{12}cm^{-2}$
Series	Characteristic curve	PQT12	$7x10^{15}cm^{-3}$	$7x10^{12}cm^{-2}$
		PQTS12	$7x10^{16}cm^{-3}$	$1x10^{12}cm^{-2}$
	Transfer I	PQT12	$7x10^{15}cm^{-3}$	$7.5x10^{12}cm^{-2}$
		PQTS12	$7x10^{16}cm^{-3}$	$1.5x10^{12}cm^{-2}$
	Transfer II	PQT12	$7x10^{15}cm^{-3}$	$7.7x10^{12}cm^{-2}$
		PQTS12	$7x10^{16}cm^{-3}$	$1.7x10^{12}cm^{-2}$

Table 2 Trap density and interface trap values used in parallel and series circuit simulations

3.2 Analyte Sensitivity Simulation

Gas analyte sensitivity is simulated and effective responses are calculated. The results are compared with the experimental data that were measured for NO_2 detection. The change in electrical characteristic due to analyte sensitivity is monitored using the doping-dependent mobility model. Experimentally, the sensing performances of the devices and circuits were investigated by exposing them to different concentrations of NO_2 in air with different exposure times and measuring Id-Vd and Id-Vg curves of the circuits [7]. The simulation equivalent of this is performing a parametric I-V simulation until the simulation and experiment match, with a doping density being a parametric variable. The mobility is extracted when the simulation matches the experiment. In both simulation and experiment, change in I_d was used to calculate the sensitivity (responsivity) of the device/circuit sensors, following the formula $(I_{d,NO2} – I_{d,air})$/

$I_{d,air}$ *100%, [7] where $I_{d,air}$ and $I_{d,NO2}$ are the drain currents before and after exposure to NO_2, respectively.

We first investigated the NO_2 responses of PQT12 and PQTS12 OFETs individually. Figure 5 shows the gas analyte sensitivity of PQT12 and PQTS12 OFETs. The changes in doping, drain current, and mobility at different NO_2 exposure times are shown in Table 3.

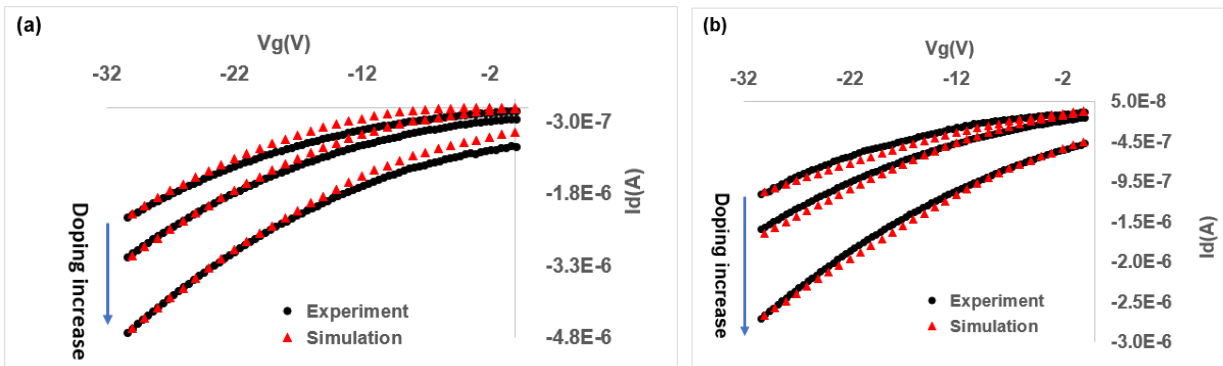

Fig.5 *Single Transistor Analyte Sensitivity Simulation (a) PQT12 and (b) PQTS12*

Response to NO_2 was modeled as an increased p-doping (hole density) compared to the unexposed devices. Figure 5 presents transfer curves for three cases of NO_2 exposure with increasing doping shown by arrows. The top curves represent transfer curves of original devises that are not exposed to NO_2. The middle ones are for devices with 1ppm 5-minute exposure to NO_2. The bottom ones are for 1ppm 10-minute exposure. The devices exposed to NO_2 are simulated by applying a change in doping level with doping-dependent mobility model. In Table 3 "change in doping" column, the zero doping indicates the base devices with no exposure to NO_2. We then changed the doping in PQT12 by 300% and in PQTS12 by 143%. The drain current increased by 34.8% and 65.9% for PQT12 and PQTS12 transistors, respectively. This matched the experimental data measured at 1ppm 5min exposure with a gate voltage of -30 V. The mobility also changed by 0.27% for PQT12 and by 1.39% for PQTS12 transistors. Similarly, analyte sensitivity simulations with 680% change in doping for PQT12 transistor and 333% change in doping for PQTS12 transistor matched with experimental data measured at 1ppm 10-minute exposure to NO_2. Mobilities are also changed accordingly as shown in Table 3.

Material	**Change in doping**	**Change in drain current**	**Change in mobility**	**Comparison with Expt.**
PQT12	0	0	0	No exposure
	300%	34.8 %	0.27%	5 min exposure at 1ppm
	680%	65.9%	0.61%	10 min exposure at 1ppm
PQTS12	0	0	0	No exposure
	143%	58.9%	1.39%	5 min exposure at 1 ppm
	333%	86.5%	3.26%	10 min exposure at 1 ppm

Table 3 Summary of results for single transistor analyte sensitivity test

Applying the same procedure, circuits simulated and matched in section 3.1.2 are tested for analyte sensitivity by applying the changes in doping and then applying the doping- dependent mobility model. Material and model parameters presented in tables 1 and 2 are used for base circuit simulation. Then the single transistor doping change that resulted in sensitivity matches to 1ppm/5-minute exposure and 1ppm/10-minute exposure are applied to test the sensitivity of the circuits. The 300% doping change for PQT12 and 143% doping change for PQTS12 are used to simulate analyte sensitivity of both parallel and series circuits at 1ppm and 5-miute exposure for NO_2. Similarly, the 680% doping change for PQT12 and 333% doping change for PQTS12 are used to simulate analyte sensitivity of both parallel and series circuits at 1ppm and 10-minute exposure. The drain-current vs drain-voltage characteristics of the parallel and series circuits are displayed in Figure 6, with extracted parameters shown in tables 4 and 5. The circuits exhibited

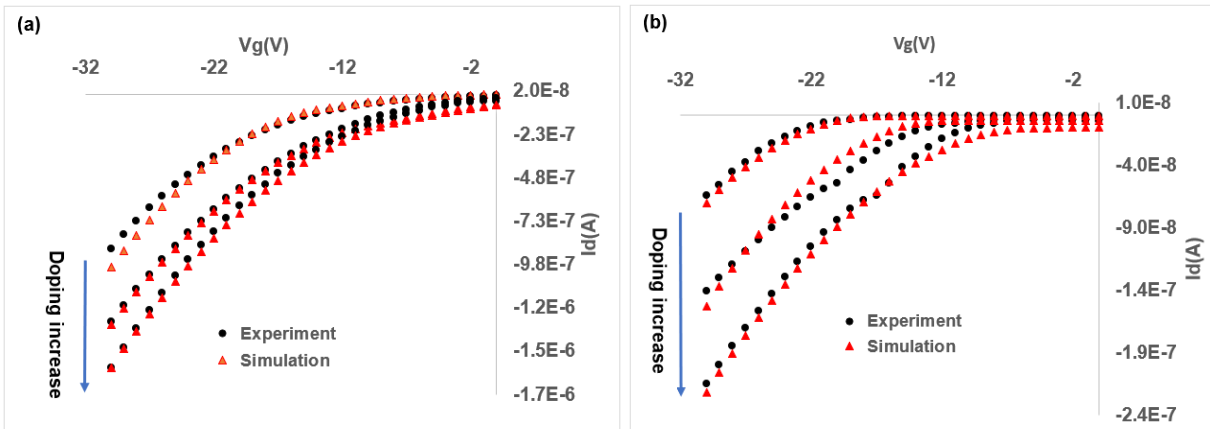

Fig.6 *(a) parallel and (b) series circuit Analyte Sensitivity Simulation*

Change in doping	**Change in drain current**	**Change in mobility**	**Comparison with Expt.**
0	0	0	No exposure
PQT12 300% **PQTS12** 143%	74.7%	0.195% 1.06%	5 min exposure at 1 ppm
PQT12 680% **PQTS12** 333%	97.8%	0.44% 2.47%	10 min exposure at 1 ppm

Table 4 Summary of results for parallel circuit analyte sensitivity test

Change in doping	**Change in drain current**	**Change in mobility**	**Comparison with Expt.**
0	0	0	No exposure
PQT12 300% **PQTS12** 143%	118%	0.267% 1.375%	5 min exposure at 1 ppm
PQT12 680% **PQTS12** 333%	227.56%	0.605% 3.21%	10 min exposure at 1 ppm

Table 5 Summary of results for series circuit analyte sensitivity test

increase in drain current (I_d) after exposure to NO_2 and show corresponding apparent mobility increases. The circuit sensors also show higher sensitivity compared to single transistor sensors for each exposure time. While the absolute value of drain currents for series circuits is lower than that of parallel circuits, the series circuit displays higher analyte sensitivity, which might be explained as the expected higher analyte sensitivity that would be obtained at lower effective gate voltage applied to the OFET nearer to the drain, which also happens to be the more sensitive (PQTS12) OFET. With exposure times of 10 minute at 1ppm, the sensitivity of parallel circuits can reach about 98% and that of series circuits can be as high as 228%. The sensitivity in terms of change in mobility is also displaying a similar trend. The series circuit shows 3.26% sensitivity while the parallel circuit is at 0.61% sensitivity with the same exposure condition to analytes. This also suggests higher sensitivity of mobility that would be obtained at lower effective gate voltage applied to the OFET nearer to the drain. Both device and circuit simulations are consistent with the experimentally observed increase in current and mobility sensitivity.

Conclusion

Organic semiconductor thin film transistors and circuits are simulated and tested for gas sensing activity. The devices are based on PQT12 and PQTS12 polymers. Two-dimensional finite element simulation methodology is implemented. Gaussian trap distributions are used in the simulation. Gas sensing is accounted for by doping dependent hopping mobility model in the organic active material. Interface traps and charges at the interface between the polymer channel and gate insulator are incorporated. Transistors in both parallel and series configurations are studied. Simulation results are compared with experiment and device parameters are extracted. Simulations are in good agreement with experiment. The results of this work demonstrate two important observations. The first one is that the experimental analyte sensitivity data for NO_2 exposure was accounted for by doping dependent mobility model in the corresponding simulation. The second observation is that two transistor circuits are confirmed to display higher sensitivity than single transistors under the same exposure conditions. This might present an opportunity for the possibility of designing high sensitivity and stabilized circuits using transistors with opposing threshold voltage shifts due to environmental effects.

Acknowledgment

We gratefully acknowledge the National Science Foundation, ECCS Division, Award Number 1087293 for supporting this work.

References

1. Dimitrakopoulos, C.D., and Mascaro, D.J.: Organic thin-film transistors: A review of recent advances, *IBM J. Res & Dev*. 45, 11 (2001).
2. Kim, H.J., Kang, S.J., Park, D.S., Chung, K.B., Noh, M., Whang, C.N., Cho, M.H.: Characterization of a Pentacene Thin-Film Transistor with a HfO_2/Al_2O_3 Gate Insulator, *Journal of the Korean Physical Society*, 45, 935 (2004)
3. Flora, L., Nathan, A., Wu, Y., Ong, B.S.: Organic Thin Film Transistor Integration: A Hybrid Approach, John Wiley & Sons (2011)
4. Yaghmazadeh, O., Cicoira, F., Bernards, D.A., Yang, S.Y., Bonnassieux, Y., Malliaras, G.G.: Optimization of Organic Electrochemical ransistors for Sensor Applications, *Journal of Polymer Science: Part B: Polymer Physics* 49, 34–39 (2011)
5. Berggren, M., Richter-Dahlfors, A.: *Adv. Mater.* 19, 3201–3213 (2007)
6. Bernards, D., Owens, R.M., Malliaras, G.G.: Organic Semiconductors in Sensor Applications, Springer: Berlin Heidelberg (2008)
7. Chu, Y., Li, H., Huang, J., Katz, H.E.: High Signal-to-Noise Chemical Sensors Based on Compensated Organic Transistor Circuits, *Advanced Materials Technologies,* 4, 10 (2019)
8. Huang, W., Sinha, J., Yeh, M.-L., Hardigree, J.F.M., LeCover, R., Besar, K., Rule, A.M., Breysse, P.N., and Katz, H.E.: *Adv. Funct. Mater*. 1-11 (2013)
9. Tremblay, N.J., Jung, B.J., Breysse, P., and Katz, H.E.: Digital-Inverter Amine Sensing via Synergistic Responses by n and p Organic Semiconductors, *Adv. Funct. Mater*. 21, 4314–4319 (2011)
10. Besar, K., Dailey, J., Zhao, X., and Katz, H.E.: A flexible organic inverter made from printable materials for synergistic ammonia sensing, *J. Mater. Chem*. C, 1- 6 (2017)
11. Bernards, D.A., and Malliaras, G.G.: Steady-State and Transient Behavior of Organic Electrochemical Transistors, *Adv. Funct. Mater*. 17, 3538–3544 (2007)
12. Donahue, M.J., Williamson, A., Strakosas, X., Friedlein, J.T., McLeod, R.R., Gleskova, H. and Malliaras, G.G: High-Performance Vertical Organic Electrochemical Transistors, *Adv. Mater*. 30, 1705031 (2018)
13. Nilsson, B.D, Chen, M., Kugler, T., Remonen, T., Armgarth, M., and Berggren, M.: *Adv. Mater.* 14, 51 (2002).
14. Robinson, N.D., Svensson, P.-Q., Nilsson, D., and Berggren, M.: *J. Electrochem. Soc*. 153, H39 (2006).
15. Friedlein, J.T., Rivnay, J., Dunlap, D.H., McCulloch, I., Shaheen, S.E., McLeod, R.R., and Malliaras, G.G.: Influence of disorder on transfer characteristics of organic electrochemical transistors, *Appl. Phys. Lett*. 111, 023301 (2017)
16. Arkhipov, V.I., Heremans, P., Emelianova, E.V., Adriaenssens, G.J., and Bässler, H.: Charge carrier mobility in doped semiconducting polymers, *Appl. Phys. Lett*. 82, 3245 (2003)
17. Pope, M., and Swenberg, C.E.: Electronic Processes in Organic Crystals and Polymers, 2nd ed. Oxford University Press, Oxford (1999)
18. Shirinskaya, A., Horowitz, G., Rivnay, J., Malliaras, G.G., and Bonnassieux, Y.: Numerical Modeling of an Organic Electrochemical Transistor, *Biosensors* 8, 103 (2018)
19. Friedlein, J.T., Shaheen, S.E., Malliaras, G.G., and McLeod, R.R.: Optical Measurements Revealing Nonuniform Hole Mobility in Organic Electrochemical Transistors, *Adv. Electron. Mater.* 1500189 (2015)
20. Vladimirov, I., Kühn, M., Geßner, T., May, F., & Weitz, R.T., Energy barriers at grain boundaries dominate charge carrier transport in an electron-conductive organic semiconductor, *Scientific Reports* 8,14868 (2018)
21. Rani, V., Sharma, A., Kumar, P., Singh, B., and Ghosh, S.: Charge transport mechanism in copper phthalocyanine thin films with and without traps, *RSC Adv.,* 7, 54911–54919 (2017)

22. Hartenstein, B., Bassler, H., Jakobs, A., and Kehr, K.W.: *Phys. Rev. B: Condens. Matter Mater. Phys.*, 54, 8574–8579 (1996).
23. Horowitz, G.: *Adv. Mater.,* 10, 365–377 (1998)
24. Vissenberg, M.C.J.M., and Matters, M.: Phys. Rev. B: *Condens. Matter Mater. Phys.,* 57, 12964–12967 (1998)
25. Guo, D., Miyadera, T., Ikeda, S., Shimada, T., and Saiki, K.: *J. Appl. Phys.,* 102, 023706 (2007)
26. Bao, Z., and Locklin, J.: Organic field-effect transistors, *CRC press* (2007).
27. Kumar, V., Jain, S., Kapoor, A., Poortmans, J., and Mertens, R.: *J. Appl. Phys*., 94, 1283–1285 (2003)
28. Agrawal, R., Kumar, P., Ghosh, S., and Mahapatro, A.K.: *Appl. Phys. Lett*., 93, 073311 (2008)
29. Lampert, M.A., and Mark, P.: Current injection in solids; Electrical science series, *Academic Press* (1970)
30. Bassler, H.: *Phys. Status Solidi B*, 175, 15–56 (1993)
31. Sharma, A., Yadav, S., Kumar, P., Chaudhuri, S.R., and Ghosh, S., *Appl. Phys. Lett*., 102, 143301 (2013)
32. Hegedus, S.S., and Fagen, E.A.: *J. Appl. Phys*., 71, 5941 (1992)
33. Sirringhaus, H.: *Adv. Mater*. 26, 1319 (2014)
34. Szymanski, M.Z., Tu, D., and Forchheimer, R.: *IEEE Transactions on Electron Devices*, 64, 12, (2017)
35. Rivnay, J., Leteux, P., Ferro, M., Sessolo, M., Williamson, A., Koutsouras, D.A., Kho, D.: "High-performance transistors for bioelectronics through tuning of channel thickness," *Sci. Adv*., 1, 4, 1400251 (2015)
36. Tu, D., Herlogsson, L., Kergoat, L., Crispin, X., Berggren, M., and Forchheimer, R.: "A static model for electrolyte-gated organic fieldeffect transistors," *IEEE Trans. Electron Devices*, 58, 10, 3574–3582 (2011)
37. Tu, D., and Forchheimer, R.: "Self-oscillation in electrochemical transistors: An RLC modeling approach," *Solid-State Electron*., 69, 7–10 (2012)
38. Coppedè, N., Villani, M., and Gentile, F.: "Diffusion driven selectivity in organic electrochemical transistors," *Sci. Rep*., 4, 4297 (2014)
39. Gentile, F., Solzi, M., Delmonte, D., Villani, M.: "A theoretical model for the time varying current in organic electrochemical transistors in a dynamic regime," *Organic Electron*., 35, 59–64 (2016)
40. Faria, G.C., Duong, D.T., and Salleo, A.: "On the transient response of organic electrochemical transistors," *Organic Electron*., 45, 215–221 (2017)
41. ATLAS User's Manual: Silvaco International, Santa Clara, CA (2007)
42. Robertson, J.: High dielectric constant oxides, *Eur. Phys. J. Appl. Phys*. 28, 265–291 (2004)
43. Giustino, F., Umari, P., Pasquarello, A.: Dielectric effect of a thin SiO2 interlayer at the interface between silicon and high-k oxides, *Microelectronic Engineering* 72, 299–303 (2004)
44. Sprague, J.L., Minahan, J.A., and Wied, O.J.: Physical and Dielectric Properties of the Metal-Silicon Dioxide-Silicon System, *Journal of the Electrochemical Society*, 109, 2, 94-98 (1962)
45. El-Kareh, B.: Silicon Devices and Process Integration: Deep Submicron and Nano-Scale Technologies by, Springer (2009)
46. Li, H., Dailey, J., Kale, T., Besar, K., Koehler, K., and Katz, H.E.: Sensitive and Selective NO2 Sensing Based on Alkyl- and AlkylthioThiophene Polymer Conductance and Conductance Ratio Changes from Differential Chemical Doping, *ACS Appl. Mater. Interfaces* 9, 20501−20507 (2017)
47. Li, H., DeCoster, M.E., Ireland, R.M., Song, J., Hopkins, P.E., and Katz, H.E.: Modification of the Poly(bisdodecylquaterthiophene) Structure for High and Predominantly Nonionic Conductivity with Matched Dopants, *Am. Chem. Soc.* 139, 32 (2017)

48. Moore, G.: IEEE Electron Devices Meeting, 11-13 (1975)
49. Rozenberg, M., Inoue , I., Sanchez, M.: Phys. Rev. Lett., 92, No. 17 (2004)
50. Pernstich, K.P., Haas, S., Oberhoff, D., Goldmann, C., Gundlach, D.J., Batlogg, B., Rashid, A.N., Schitter, G.: Threshold Voltage Shift in Organic Field Effect Transistors by Dipole Monolayers on the Gate Insulator. *J. Appl. Phys.* 96, 6431−6438 (2004)